UC Berkeley
UC Berkeley Previously Published Works

Title
Influence of stoichiometry on the dielectric properties of sputtered strontium titanate thin films

Permalink
https://escholarship.org/uc/item/9292s4pm

Journal
Journal of Applied Physics, 94(5)

ISSN
0021-8979

Authors
Taylor, T R
Hansen, P J
Pervez, N
et al.

Publication Date
2003-09-01

Peer reviewed

eScholarship.org Powered by the California Digital Library
University of California

JOURNAL OF APPLIED PHYSICS VOLUME 94, NUMBER 5 1 SEPTEMBER 2003

Influence of stoichiometry on the dielectric properties of sputtered strontium titanate thin films

T. R. Taylor and P. J. Hansen
Department of Materials, College of Engineering, University of California, Santa Barbara, California 93106

N. Pervez, B. Acikel, and R. A. York
Department of Electrical and Computer Engineering, College of Engineering, University of California, Santa Barbara, California 93106

J. S. Speck[a)]
Materials Department, College of Engineering, University of California, Santa Barbara, California 93106

(Received 26 March 2003; accepted 12 June 2003)

The dielectric permittivity, dielectric quality factor (inverse dielectric loss), and lattice parameter of 140 nm sputtered $SrTiO_3$ films were dependent on the oxygen partial pressure and total chamber pressure (O_2+Ar) during film growth. Films were grown at 25 and 75 mTorr (mT) in an oxygen rich and oxygen deficient sputtering gas environment concurrently on (100) $SrTiO_3$ and (111) Pt/(0001) Al_2O_3 substrates. Films were deposited on platinized sapphire for electrical characterization and the homoepitaxial films were used as a structural and chemical standard. High resolution triple axis x-ray diffraction results showed an increase in mismatch between the film and substrate (200) peak in homoepitaxial $SrTiO_3$ films with higher total growth and lower oxygen pressures. Dielectric quality factors of the $SrTiO_3$ films on platinized sapphire at 1 MHz for the 25 mT (50 sccm Ar/50 sccm O_2), 25 mT (90 sccm Ar/10 sccm O_2), 75 mT (50 sccm Ar/50 sccm O_2), and 75 mT (90 sccm Ar/10 sccm O_2) film growths were 320, 251, 209, and 102, respectively; likewise, the dielectric constants follow as 241, 230, 220, and 170, respectively. Improved film dielectric properties were observed for films closer to stoichiometric $SrTiO_3$. © *2003 American Institute of Physics.* [DOI: 10.1063/1.1598274]

INTRODUCTION

$SrTiO_3$ thin films have been widely studied for their high dielectric constants and potential application as the charge storage material in high density dynamic random access memories (DRAMs).[1] $SrTiO_3$ is also an incipient ferroelectric that has low dielectric loss and large dielectric nonlinearity at cryogenic temperatures. This makes it an ideal candidate for tunable microwave devices with high temperature superconductors. The dielectric permittivity of $SrTiO_3$ thin films is significantly smaller than the bulk form. Various reasons have been proposed for the difference in dielectric constant including dead-layer effects, interfacial reactions, and film stress.[2,3]

(Ba,Sr)TiO_3 thin films are currently of great interest because of their room temperature field-dependent dielectric constant and possible application in microwave circuits.[4] $SrTiO_3$ and (Ba,Sr)TiO_3 thin films have the potential to compete with GaAs-based Schottky diodes in microwave varactor technology;[5] therefore, a highly insulating substrate is required for reduced losses. For our work, sapphire was chosen because it is a large area, low cost substrate with a low loss tangent. Furthermore, Pt deposition on sapphire is well developed and less challenging than Pt integration with silicon.[6] Although $SrTiO_3$ does not have large dielectric tunability at room temperature, it does have a large dielectric quality factor and simplified structural characterization because of the possibility of homoepitaxial growth on $SrTiO_3$ substrates. Recently we investigated the role of thermal strain on the dielectric constants of (Ba,Sr)TiO_3 thin films and saw a reduction in dielectric permittivity with an increase in thermal tensile strain.[7] In this article we investigate the impact of nonstoichiometry on the dielectric properties of $SrTiO_3$ thin films.

EXPERIMENTAL PROCEDURE

$SrTiO_3$ thin films were grown concurrently on (100) $SrTiO_3$, (0001) Al_2O_3, and platinized (0001) Al_2O_3 substates. Films were deposited by rf magnetron sputtering from two 3 in. $SrTiO_3$ targets (99.99% purity) at a power density of 21.25 W/in.^{2}. Sources in the growth chamber were 30° off axis with a 4.25 in. source to substrate distance. Each sample had a 500 nm backside titanium layer deposited by electron beam evaporation for heat absorption. Acetone/isopropanol and trichloroethane/acetone/isopropanol were used to clean the sapphire and $SrTiO_3$ substrates, respectively, followed by a 10 min bake at 115 °C. Growth as was carried out either at 25 or 75 mT at 700 °C surface temperature with varying oxygen and argon pressures by changing their respective flow rates. Films grown on (0001) sapphire were analyzed by Rutherford backscattering spectroscopy (RBS) to determine their thickness and composition.

Parallel plate capacitors were fabricated on the $SrTiO_3$/Pt/Al_2O_3 samples by a two-step mask process. An

[a)]Electronic mail: speck@mrl.ucsb.edu

 © 2003 American Institute of Physics

Downloaded 21 Sep 2003 to 128.111.74.212. Redistribution subject to AIP license or copyright, see http://ojps.aip.org/japo/japcr.jsp

TABLE I. Sputtering conditions and $SrTiO_3$ surface roughness.

Pressure (mTorr)	Ar flow (sccm)	O_2 flow (sccm)	Growth rate (A/min)	Roughness (rms) (Å)
25	90	10	15	3.01
25	50	50	12	5.00
75	90	10	9	24.2
75	50	50	7	27.6

etch mask defined the active dielectric area, and the 100 nm thick Pt top contacts were patterned by a lift-off process. Pt top contacts were deposited by electron beam evaporation at room temperature. The 100 nm thick Pt bottom electrode was deposited by rf magnetron sputtering from a 3 in. Pt target. Sputtering was done at 25 mTorr (100 sccm Ar) and a 600 °C surface temperature. Prior to electrical measurements an anneal was done at 600 °C in flowing oxygen (75 sccm O_2) at atmospheric pressure. An Agilent 4294A variable frequency (40–110 MHz) impedance analyzer was used to characterize the capacitors with a 200 mV oscillating electric field. Leakage currents were measured using a Keithley 6517A electrometer as a voltage source and ammeter, along with series resistance of 110 MΩ to limit current in the event of a short circuit. The data presented here account for the series resistance as well as for any current measurement offset, the presence of which was determined by measuring the depolarization current as a function of time after the voltage sweep returned to zero.

Atomic force microscopy (AFM) and triple-axis x-ray diffraction were used to investigate homoepitaxial $SrTiO_3$ films. The effect of growth parameters on the film was determined by comparing the (200) peak separation between the $SrTiO_3$ substrate and film deposited using a Philips Materials Research diffractometer (MRD PRO) with ~10 arcsec resolution. The film strain was determined from the peak separation. Films deposited at both 25 and 75 mT were grown in two distinct sputtering gas regimes by varying the sputtering gas ratios. $SrTiO_3$ films were sputtered in an oxygen rich (50 sccm Ar/50 sccm O_2) and oxygen deficient (90 sccm Ar/10 sccm O_2) environment, as detailed in Table I. The deposition rate decreased with reduced argon flow and increased oxygen flow because of the relative decrease of argon species contributing to the sputter yield, as verified by RBS.[8]

RESULTS

A preliminary growth study was performed on (100) $SrTiO_3$ and (0001) Al_2O_3 substrates at total growth pressures of 25 and 75 mT and with two different O_2/Ar ratios at each growth pressure. The homoepitaxial $SrTiO_3$ films were characterized by AFM and x-ray diffraction, while the $SrTiO_3$ films grown on sapphire samples were analyzed by RBS. AFM images of the 25 mT films in Figs. 1(a) and 1(b) show the effect of oxygen on the film surface morphology. Step flow growth was evident in the 128 nm thick sample grown at 25 mT (90 sccm Ar/10 sccm O_2) and had a root mean square (rms) roughness of ~3 Å. The 103 nm thick oxygen rich sample at 25 mT (50 sccm Ar/50 sccm O_2) displayed a rougher surface, a rms roughness of 7–8 Å. The rougher surface was attributed to lower cation mobility on the growth surface with higher oxygen pressures. The film thickness and Sr/Ti composition were determined by RBS. Both films were found to be titanium deficient with a Sr/Ti ratio of 1.02. Homoepitaxial films grown at 75 mT (90 sccm Ar/10 sccm O_2), 75 mT (70 sccm Ar/30 sccm O_2), and 75 mT (50 sccm Ar/50 sccm O_2) had Sr/Ti ratios of 1.40, 1.19, and 1.02, respectively.

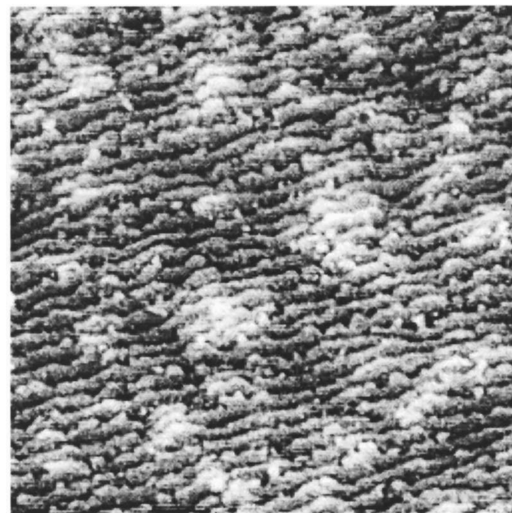

(a)

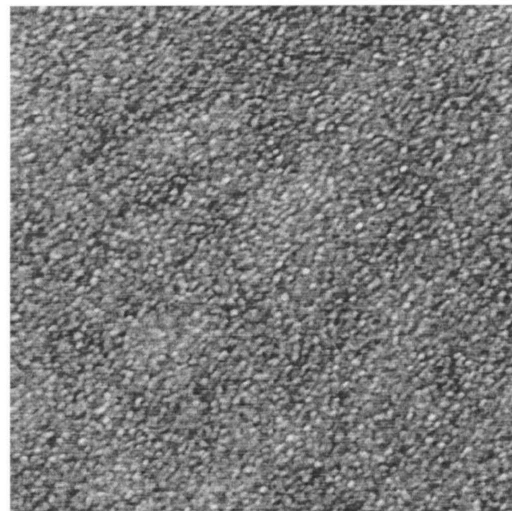

(b)

FIG. 1. (a) AFM image of $SrTiO_3$ homoepitaxy at 25 mT: 90 sccm Ar/10 sccm O_2 (0.5 μm×0.5 μm). (b) AFM image of $SrTiO_3$ homoepitaxy at 25 mT: 50 sccm Ar/50 sccm O_2 (3 μm×3 μm).

Another set of samples was grown concurrently on (100) $SrTiO_3$, (0001) Al_2O_3, and platinized (0001) Al_2O_3 at 25 mT (90 sccm Ar/10 sccm O_2), 25 mT (50 sccm Ar/50 sccm O_2), 75 mT (90 sccm Ar/10 sccm O_2), and 75 mT (50 sccm Ar/50 sccm O_2). Growth was carefully monitored to ensure that each sample was of equal thickness because the dielectric constant of barium strontium titanate thin films on plati-

Downloaded 21 Sep 2003 to 128.111.74.212. Redistribution subject to AIP license or copyright, see http://ojps.aip.org/japo/japcr.jsp

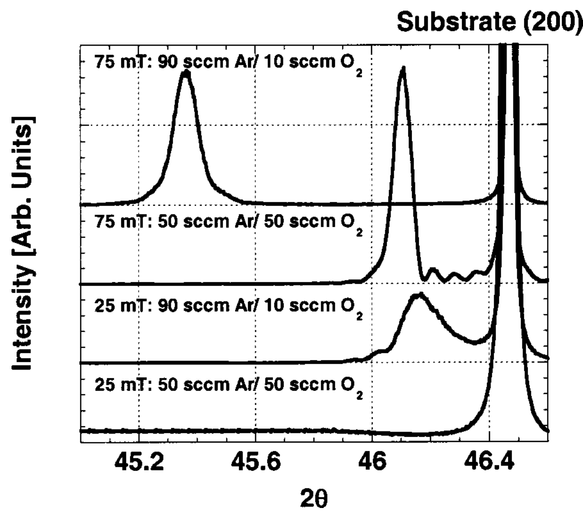

FIG. 2. Triple axis x-ray diffraction scans, 2θ–ω, of $SrTiO_3$ homoepitaxial films with the different sputtering conditions noted.

num electrodes is thickness dependent.[3] RBS analysis confirmed equal thickness films of 140 nm with compositions in agreement with the previous series. Triple axis x-ray diffraction scans, ω–2θ, were performed on the homoepitaxial films. Scans were done of the (200) $SrTiO_3$ peak to observe any splitting between the film and substrate peaks. Figure 2 shows x-ray scans of the samples. The (200) peak for the oxygen deficient 25 mT (90 sccm Ar/10 sccm O_2) film was shifted towards lower 2θ values with respect to the substrate, while the oxygen rich film grown at the same pressure did not display a split peak. A larger peak separation was seen with the higher pressure, 75 mT, samples. The (200) film peak shifted towards lower 2θ values, demonstrating that the out-of-plane lattice parameter of the film is larger than the substrate. The measured full width at half maximum (FWHM) values for ω–2θ scans of the (200) $SrTiO_3$ films that displayed a separate film peak by triple axis diffraction were between 220 and 230 arcsec, which is in good agreement for the calculated broadening of a 140 nm (200) $SrTiO_3$ film of ~222 arcsec.[9] Visible pendellosung fringes in the ω–2θ scans corresponded to approximately a 140 nm film thickness.[10,11]

Rocking curves (ω scans) were performed for the samples that had a split (200) film peak to determine if the films were fully coherent. Symmetric, on-axis (200) rocking curves of the film and substrate were normalized for comparison to investigate strain relaxation. The normalized rocking curves were nearly identical thus indicating that strain relaxation through the generation of misfit dislocations had not occurred in the films. Asymmetric, off-axis (310) rocking curves for the 75 mT (90 sccm Ar/10 sccm O_2) sample confirmed a coherent film with the in-plane film lattice parameters (a_x, a_y) equal to the substrate (a_s). The out-of-plane film lattice parameter (a_z) has been determined directly from on-axis ω–2θ scans of the (200) film peaks that show a distorted a_z lattice parameter due to unrelaxed compressive biaxial strain. From Eq. (1) the intrinsic cubic film lattice parameter (a_f) can be determined, while the biaxial strain

TABLE II. Calculated growth stresses from (002) peak separation.

P_{total} (mTorr)	Ar/O_2 (sccm)	$\Delta 2\theta$ (deg)	a_z (Å)	a_f (Å)	ε_{xx} (%)	σ (GPa)
25	90/10	0.31	3.929	3.920	−0.37	−0.90
75	90/10	1.12	3.993	3.960	−1.4	−3.45
75	50/50	0.37	3.933	3.922	−0.44	−1.10

(ε_{xx}) and stress (σ) of the film are given in Eqs. (2a) and (2b) since the film is coherent.

$$a_f = \frac{[(1-\nu)a_z + (2\nu)a_s]}{(1+\nu)}, \tag{1}$$

$$\varepsilon_{xx} = \frac{a_s - a_f}{a_f}, \tag{2a}$$

$$\sigma = \frac{[(a_s - a_f)E]}{(1-\nu)a_f}. \tag{2b}$$

For bulk single crystal $SrTiO_3$, $a_s = 3.905$ Å, E (the Young's modulus) = 189.7 GPa, and ν (the Poisson ratio) = 0.232.[12] The calculated film parameters and related strains are summarized in Table II.

Zero-bias capacitance and quality factors were measured on the processed $SrTiO_3$ capacitors on platinized sapphire. The (0001) sapphire substrates had 100 nm of Pt deposited by sputtering at a 600 °C surface temperature. Figure 3 shows a (200) Pt pole figure that displays sixfold {111} Pt texture at 54.7° in accordance with the (0001) Al_2O_3 substrate. High resolution triple axis diffraction ω–2θ scans determined FWHM values of 310 arcsec for the (111) Pt peak which is in good agreement with the calculated broadening of a 100 nm Pt film of ~304 arcsec.[9] Rocking curve measurements of the (111) epitaxial platinum had a FWHM of 200 arcsec. The rms surface roughness of the Pt film on sapphire was found to be 3 Å by AFM.[13] X-ray diffraction measurements, θ–2θ, of $SrTiO_3$ films grown on platinized sapphire found (100) and (110) peaks that displayed rocking

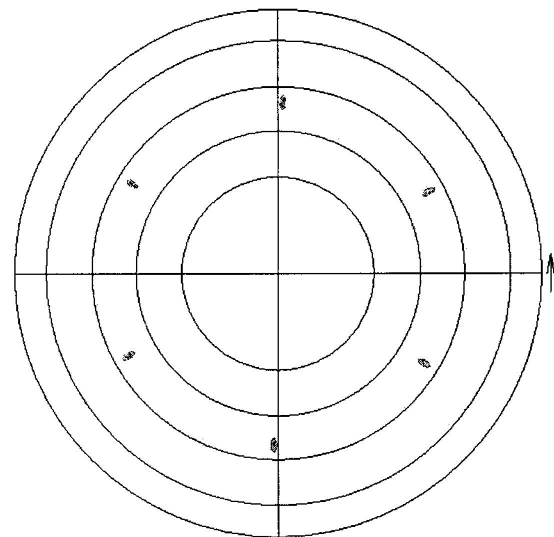

FIG. 3. (200) Pt pole figure for 100 nm thick Pt films deposited on (0001) Al_2O_3.

Downloaded 21 Sep 2003 to 128.111.74.212. Redistribution subject to AIP license or copyright, see http://ojps.aip.org/japo/japcr.jsp

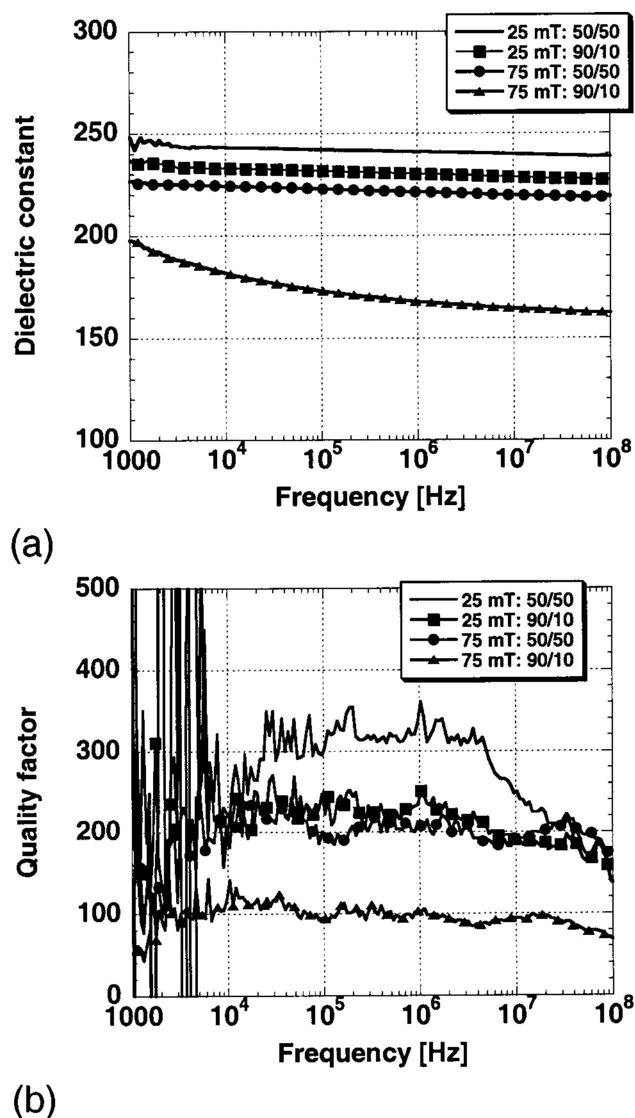

FIG. 4. (a) Frequency dependent dielectric constant of 140 nm thick $SrTiO_3$ films on platinized sapphire (see the inset for growth conditions). (b) Quality factor vs frequency for $SrTiO_3$ devices on a 100 nm thick Pt bottom electrode.

curve FWHM values from 0.5° to 0.8°. The (111) $SrTiO_3$ peak could not be directly measured due to the strong signal from the (111) Pt peak. Preliminary plane view transmission electron microscopy (TEM) results show that films on platinized sapphire have predominantly (110) and (111) textures.[14]

Figures 4(a) and 4(b) show the measured film dielectric constant and quality factor as a function of the frequency. These results show a clear trend of improved film electrical properties when the concurrently grown homoepitaxial film is under less compressive biaxial strain. The $SrTiO_3$ film grown at 25 mT (50 sccm Ar/50 sccm O_2) revealed no split peak, and the film grown simultaneously on platinized sapphire yielded the highest dielectric constant (241) and largest dielectric quality factor (320) at 1 MHz. The $SrTiO_3$ film grown at 75 mT (90 sccm Ar/10 sccm O_2) was calculated to be under compressive strain of 1.4% and its platinized sapphire counterpart produced the lowest dielectric constant (170) and worst quality factor (102) at 1 MHz. A leakage component that contributes to the measured capacitance at low frequencies (10^3-10^5 Hz) may be responsible for the larger dispersion in the dielectric constant for the 75 mT (90 sccm Ar/10 sccm O_2) $SrTiO_3$ film in comparison to the other samples. Leakage current measurements performed on 75 mT (90 sccm Ar/10 sccm O_2) and 75 mT (50 sccm Ar/50 sccm O_2) showed the samples reached a current density of 100 nA/cm^2 at 2 and 6 V, respectively.

DISCUSSION

The collision dynamics in a plasma and its energetic ions complicate stoichiometric film growth by sputtering. Sigmund described sputtering as a collision cascade with an energetic flux of sputtered species moving towards a substrate.[15] Gas phase scattering during the sputtering process is mass dependent.[16,17] Sputtered species with masses similar to ambient gases (Ar and O_2) have a higher probability of being scattered from their original trajectory. During growth, heavier elements travel towards the substrate with lower angular dispersion. For $SrTiO_3$ the atomic masses are as follows: $m_{Sr}=88$, $m_{Ti}=48$, $m_{O_2}=32$, and $m_{Ar}=40$. The Ti atoms are scattered less when the Ar flow and total sputtering pressure are reduced during growth. Bombardment of the film by energetic ions created by sputtering can also affect film stoichiometry and strain. Resputtering processes can occur when the film is bombarded by energetic species as has been observed in the growth of $YBa_2Cu_3O_{7-x}$.[18] Oxygen loss has been documented in TiO_2 when it is bombarded by ions with energy of at least 6.4 eV.[19] The activation enthalpy for creating an oxygen vacancy (V_O'') in $SrTiO_3$ is approximately 5.76 eV.[20] Ion bombardment should be considered a source for generating oxygen vacancies since particle energy distributions in rf magnetron sputtering are typically 1–10 eV.[21,22]

Physical vapor deposition growth techniques result in large strain during film growth. High resolution triple axis diffraction has shown that the strain in homoepitaxial $SrTiO_3$ thin films is dependent on the sputtering growth parameters including the total growth pressure and oxygen partial pressure. Homoepitaxial growth of single crystal films eliminates thermal mismatch, lattice misfit, grain boundary coalescence, and solid state reactions/interdiffusion as appreciable sources of strain.[23] Films were grown concurrently on different substrates so they experienced different growth modes, but the same flux impinged on each substrate surface. The observed separation of the $SrTiO_3$ film (200) peak from the substrate is created by film nonstoichiometry. RBS data have shown that the films are titanium deficient by having a Sr/Ti ratio greater than 1. In complex oxide material systems, oxygen point defect concentrations are also affected by cation stoichiometry.[24,25] Physical vapor deposition techniques such as sputtering and laser ablation can impact the film composition because of mass and pressure dependent gas scattering processes; therefore, film stoichiometry is a function of the growth pressure.[16,26] The film grown at 25 mT and higher oxygen pressure (50 sccm Ar/50 sccm O_2) is closer to stoichiometric $SrTiO_3$ because no split peak was observed in

Downloaded 21 Sep 2003 to 128.111.74.212. Redistribution subject to AIP license or copyright, see http://ojps.aip.org/japo/japcr.jsp

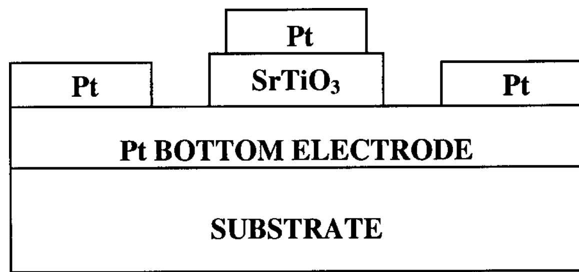

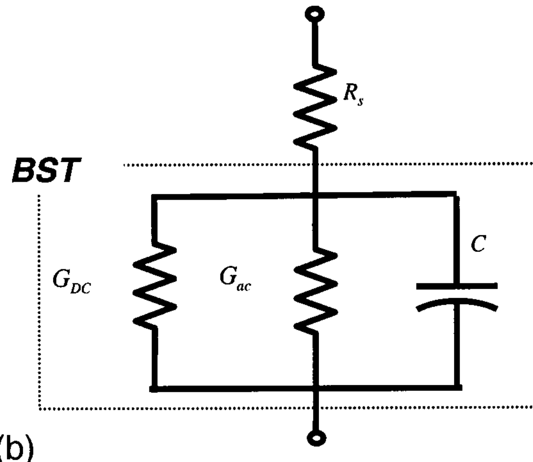

FIG. 5. (a) $SrTiO_3$ capacitor structure on a sapphire substrate. (b) Circuit diagram of the $SrTiO_3$ capacitor structure.

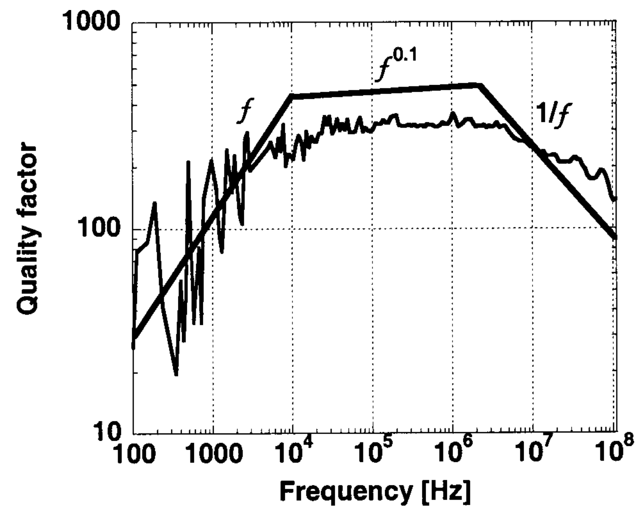

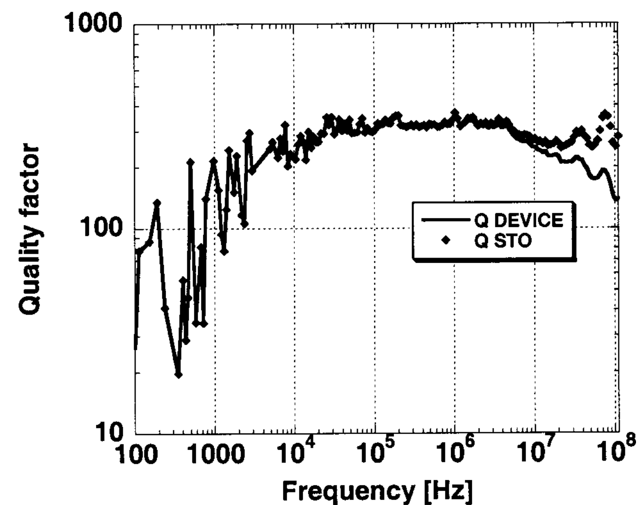

FIG. 6. (a) Total device quality factor as a function of the frequency (f). (b) Measured total device and extracted $SrTiO_3$ film quality factor for $SrTiO_3$ film grown at 25 mT: 50 sccm Ar/50 sccm O_2 (140 nm $SrTiO_3$ and 100 nm Pt films).

the x-ray diffraction. The data suggest that higher sputtering pressures impede the growth of stoichiometric films, but oxygen rich growth environments promote stoichiometric film growth. Similar results have been reported for $SrTiO_3$ thin films deposited by laser ablation.[27]

The quality factor was used to characterize the loss in a circuit.[28,29] Figures 5(a) and 5(b) show the capacitor structure and equivalent circuit diagram of the $SrTiO_3$ devices. Measured capacitors were 30 μm$\times$50 μm with 50 μm pitch. R_S, G_{dc}, G_{ac}, and C represent the series resistance from the contact electrodes, conductance as a result of dc leakage from free/mobile charge, conductance due to dielectric loss, and the capacitance, respectively. The total quality factor for the $SrTiO_3$ device in terms of individual components is shown in Eqs. (3) and (4a)–(4c) where ω is the angular frequency. Figure 6(a) shows the frequency dependence of the total device quality factor (Q_{total}).

$$\frac{1}{Q_{\text{total}}}=\frac{1}{Q_{\text{leakage}}}+\frac{1}{Q_{\text{SrTiO}_3}}+\frac{1}{Q_{\text{Pt}}}, \tag{3}$$

$$Q_{\text{leakage}}=\frac{\omega C}{G_{\text{dc}}}, \tag{4a}$$

$$Q_{\text{SrTiO}_3}=\frac{\omega^n C}{G_{\text{ac}}}, \tag{4b}$$

$$Q_{\text{Pt}}\sim\frac{1}{\omega R_s C}. \tag{4c}$$

At low frequencies Q_{leakage} dominates the device quality factor [Eq. (4a)]. Q_{leakage} increases linearly with the frequency and losses in leakage increase with bias applied. Nonstoichiometric films have increased leakage losses because of the larger concentration of free carriers, electrons, from oxygen vacancies that increase film conductivity.[30,31] In ionic lattices polaron conduction can contribute to leakage currents where electrons can move in the conduction band (large polaron) or from site to site by thermally activated hopping (small polaron).[32,33] Reduced bulk $SrTiO_3$ samples have been shown to have conductivities as high as 10^{-1} $(\Omega\,\text{cm})^{-1}$ and increased loss tangents.[25] The $SrTiO_3$ film conductivity cannot be directly determined from the thin film capacitors because of interfacial resistance from the Pt Schottky contact. Leakage current measurements suggest higher electron doping and stronger n-type behavior in the 75 mT film grown at lower oxygen pressures. Oxygen vacancies have a defect level approximately 0.3 eV below

Downloaded 21 Sep 2003 to 128.111.74.212. Redistribution subject to AIP license or copyright, see http://ojps.aip.org/japo/japcr.jsp

the conduction band edge and act as shallow donors.[31] Insufficient oxygen pressure during growth results in the formation of oxygen vacancies $[O_O \rightarrow V_O'' + 2_e'' + 0.5O_2(g)]$ and larger leakage currents.[34]

For intermediate frequencies the device quality factor is determined by the conductance associated with dielectric loss in the $SrTiO_3$ film [Eq. (4b)]. Energy loss from dipole relaxation mechanisms must be considered in the loss tangent for oxygen deficient $SrTiO_3$. Oxygen vacancies distort the lattice thus lowering its crystal symmetry and can act as dipole centers that interact with an applied ac electric field thereby contributing to dielectric loss.[2] The intermediate regime has a power law frequency dependence (ω^n) that is not well understood[35] and was experimentally determined to have $n \sim 0.1$.

At high frequencies the platinum bottom electrode dominates the total device quality factor [Eq. (4c)]. Figure 6(b) shows the total device quality factor and the extracted quality factor for the $SrTiO_3$ film deposited at 25 mTorr (90 sccm Ar/10 sccm O_2). The $SrTiO_3$ film quality factor was determined by separating it from the conductor losses associated with the Pt bottom electrode. The measured series resistance of shorted capacitor structures revealed an extracted Pt resistivity of $\sim 12\ \mu\Omega\,\mathrm{cm}$ in good agreement with the bulk resistivity of Pt ($\sim 10.6\ \mu\Omega\,\mathrm{cm}$). The $SrTiO_3$ film quality factor remains constant with an increase in frequency even as the total device quality factor decreases due to conductor losses. Thicker base electrodes could be used to reduce the series resistance associated with the varactor and minimize conductor losses.[28]

In an ideal ferroelectric crystal the microwave loss is associated with dampening of a low frequency traverse optical phonon or soft mode.[2,36] The origin of intrinsic loss is the interaction of an applied ac field with the phonons of the dielectric. It has been well established by Gurevich and Tagantsev that there are three mechanisms responsible for the intrinsic dielectric loss in crystals: three quantum, four quantum, and quasi-Debye.[36] All of these mechanisms are associated with multiple phonon absorption, and the quasi-Debye mechanism only occurs in noncentrosymmetric crystals. The microwave frequencies are smaller than the soft mode for $SrTiO_3$ ($\omega_{TO} = 2.7$ THz); therefore, field absorption results in the transition between different phonon branches such as two soft mode phonons or a soft mode and an acoustic phonon.[36] When a defect is present in the material additional loss mechanisms become possible because of phonons localized at the defect. One phonon absorption mechanisms become possible as the defect and neighboring atoms respond to the microwave field and result in the emission of acoustic phonons and increased dielectric loss.[2,36] Dielectric loss is affected by direct loss, the emission of phonons from uncharged defects, and phonon–defect interactions or indirect loss for charged defects. Theoretical calculations by Gurevich and Tagantsev from phonon theory are in good agreement with the measured loss tangent for several single crystal dielectrics (NaCl, $SrTiO_3$, and Al_2O_3),[36] although dielectric and ferroelectric thin films offer a more complicated problem with many unsolved experimental and theoretical problems. Thin film growth methods such as sputtering lead to a wide variety of point defects and additional extended defects such as dislocations and grain boundaries. Many of these imperfections stem from the process requirements for device integration that set growth temperature limitations and yield polycrystalline films. It is clear that substantial further effort is required to understand point defect related microwave loss mechanisms.

CONCLUSION

In summary, high resolution triple axis x-ray diffraction was used to investigate growth stress in homoepitaxial $SrTiO_3$ films. The (200) peak splitting between the substrate and the film was found to depend on the total growth and oxygen pressure. RBS confirmed that the films were Ti deficient, but the Sr/Ti ratio was close to 1 at lower total growth pressures with higher oxygen fraction. Nonstoichiometry in complex oxides such as $SrTiO_3$ and $BaTiO_3$ leads to a strained lattice parameter that is measured as tetragonal distortion. Films grown concurrently on platinized sapphire were fabricated into capacitors and tested for their electrical characteristics. Homoepitaxial films under less compressive biaxial strain were closer to stoichiometry and films concurrently grown on platinized sapphire had higher dielectric constants and better dielectric loss performance. Dielectric loss is dominated by extrinsic factors such as oxygen vacancies and conductivity as opposed to phonon limited intrinsic loss mechanisms. Films deposited by sputtering are grossly nonstoichiometric and this is a major reason for the order of magnitude difference between loss tangents for thin films ($10^{-3}-10^{-2}$) and bulk samples ($10^{-4}-10^{-3}$). Future studies should investigate the microstructure of nonstoichiometric dielectric films and their dielectric properties.

ACKNOWLEDGMENTS

This research was supported by DARPA through the Frequency Agile Materials for Electronics Program (FAME) under Award No. DABT63-98-1-0006. Sputtering system fabrication was supported by the Army Research Office (ARO) through DURIP equipment Award No. DAAD19-99-1-0060. This work made use of the MRL Central Facilities supported by the National Science Foundation under Award No. DMR 96-32716. RBS analysis was done by the Ion Beam Facility of CCMR, Cornell University, supported through NSF Grant No. DMR-963227.

[1] C. S. Hwang, S. O. Park, C. S. Kang, H. Cho, H. Kang, S. T. Ahn, and M. Y. Lee, Jpn. J. Appl. Phys., Part 1 **34**, 5178 (1995).
[2] H. C. Li, W. Si, A. D. West, and X. X. Xi, Appl. Phys. Lett. **73**, 464 (1998); X. X. Xi, H. C. Li, W. Si, A. A. Sirenko, I. A. Akimov, J. R. Fox, A. M. Clark, and J. Hao, J. Electroceram. **4**, 393 (2000).
[3] S. K. Streiffer, C. Basceri, C. B. Parker, S. E. Lash, and A. I. Kingon, J. Appl. Phys. **86**, 4565 (1999).
[4] E. G. Erker, A. S. Nagra, Y. Liu, P. Periaswamy, T. R. Taylor, J. S. Speck, and R. A. York, IEEE Microw. Guid. Wave Lett. **10**, 10 (2000).
[5] A. S. Nagra and R. A. York, IEEE Trans. Microwave Theory Tech. **47**, 1705 (1999).
[6] E. A. Kneer, D. P. Birnie, R. D. Schrimpf, J. C. Podlesny, and G. Teowee, Integr. Ferroelectr. **7**, 61 (1995).
[7] T. R. Taylor, P. J. Hansen, B. Acikel, N. Pervez, S. K. Streiffer, R. A. York, and J. S. Speck, Appl. Phys. Lett. **80**, 1978 (2002).

Downloaded 21 Sep 2003 to 128.111.74.212. Redistribution subject to AIP license or copyright, see http://ojps.aip.org/japo/japcr.jsp

[8] M. Ohring, *The Materials Science of Thin Films* (Academic, New York, 1991).
[9] B. D. Cullity, *Elements of X-Ray Diffraction* (Addison–Wesley, Reading, MA, 1978).
[10] B. E. Warren, *X-Ray Diffraction* (Dover, New York, 1969).
[11] G. Bauer and W. Richter, *Optical Characterization of Epitaxial Semiconductor Layers* (Springer, Berlin, 1996).
[12] H. Ledbetter, M. Lei, and S. Kim, Phase Transitions **23**, 61 (1990).
[13] Unpublished results; see the following for similar results: R. F. C. Farrow, G. R. Harp, R. F. Marks, T. A. Radebeau, M. F. Toney, D. Weller, and S. S. P. Parkin, J. Cryst. Growth **133**, 47 (1993).
[14] D. O. Klenov, T. R. Taylor, J. S. Speck, and S. Stemmer (unpublished).
[15] P. Sigmund, Phys. Rev. **184**, 383 (1969).
[16] G. K. Werner, J. Vac. Sci. Technol. A **1**, 487 (1983).
[17] J. Im, O. Auciello, P. K. Baumann, S. K. Streiffer, D. Y. Kaufman, and A. R. Krauss, Appl. Phys. Lett. **76**, 625 (2000).
[18] M. Migliuolo, R. M. Belan, and J. A. Brewer, Appl. Phys. Lett. **56**, 2572 (1990).
[19] R. Kelly, Surf. Sci. **100**, 85 (1980).
[20] J. F. Scott, S. A. T. Redfern, M. Zhang, and M. Dawber, J. Eur. Ceram. Soc. **21**, 1629 (2001).
[21] J. J. Cuomo, D. L. Pappas, J. Bruley, J. Doyle, and K. L. Saenger, J. Appl. Phys. **70**, 1706 (1991).
[22] D. Smith, *Thin-Film Deposition* (McGraw–Hill, New York, 1995).
[23] R. Koch, J. Phys.: Condens. Matter **6**, 9519 (1994).
[24] M. J. Akhtar, Z. Akhtar, R. A. Jackson, and C. R. A. Catlow, J. Am. Ceram. Soc. **78**, 421 (1995).
[25] N. H. Chan, R. K. Sharma, and D. M. Smyth, J. Electrochem. Soc. **128**, 1762 (1981).
[26] J. Gonzalo, C. N. Afonso, and J. Pierrere, Appl. Phys. Lett. **67**, 1325 (1995).
[27] E. J. Tarsa, E. A. Hachfeld, F. T. Quinlan, J. S. Speck, and M. Eddy, Appl. Phys. Lett. **68**, 490 (1996).
[28] D. Pozar, *Microwave Engineering* (Wiley, New York, 1998).
[29] A. J. Moulson and J. M. Herbert, *Electroceramics* (Chapman and Hall, London, 1990).
[30] M. S. Tsai, S. C. Cun, and T. Y. Tseng, J. Appl. Phys. **82**, 3482 (1997).
[31] D. E. Kotecki, IBM J. Res. Dev. **43**, 367 (1999).
[32] W. D. Kinery, H. K. Bowen, and D. R. Uhlmann, *Introduction to Ceramics* (Wiley, New York, 1960).
[33] W. A. Harrison, *Solid State Theory* (Dover, New York, 1979).
[34] Y. Fukuda, H. Haneda, I. Sakaguchi, K. Numata, K. Aoki, and A. Nishimura, Jpn. J. Appl. Phys., Part 2 **36**, L1514 (1997).
[35] A. K. Jonscher, J. Phys. D **32**, R57 (1999).
[36] V. L. Gurevich and A. K. Tagantsev, Adv. Phys. **40**, 719 (1991).

Downloaded 21 Sep 2003 to 128.111.74.212. Redistribution subject to AIP license or copyright, see http://ojps.aip.org/japo/japcr.jsp